Detection of Magnetic Particles by Magnetoresistive Sensors

A. Weddemann,* A. Auge, F. Wittbracht, C. Albon, and A. Hütten
Department of Physics, Thin Films and Physics of Nanostructures, Bielefeld University
*Universitätsstr. 25, 33615 Bielefeld, Germany, *weddeman@physik.uni-bielefeld.de*

Abstract: In this work, we demonstrate the implementation of the micromagnetic equations for the description of ferromagnetic thin films in COMSOL Multiphysics. We apply our model to magnetoresistive sensors consisting of several soft ferromagnetic layers and their response to magnetic particles. The magnetization dynamic of the particles needs to be described in a similar manner, though due to size effects it is possible to reduce the description to a set of ordinary differential equations. The signal will be discussed in respect to the particle position as well as the influence of antiferromagnetic ordering in particle clusters that are within detection range.

Keywords: ferromagnetism, micromagnetism, magnetic particles, magnetoresistive sensors

1. Introduction

Magnetic particles have gained a lot of interest in lab-on-a-chip applications during the last decades.[1,2] Their magnetic moment enables their manipulation[3,4] by external magnetic fields and due to their stray field they themselves influence magnetic material close to them. The latter effect can be exploited for the detection of particles by magnetoresistive sensors,[5] which consist (in the simplest setting) of two ferromagnetic electrodes separated by a non-magnetic (insulating or conducting) spacer layer. The resistance of this layer stack varies depending on the relation between the orientation of the magnetization distribution in each of the layers. Generally, a parallel alignment leads to a small, an antiparallel state to a high resistance. A proper understanding of the measured resistance change requires detailed knowledge of the underlying dynamics. In this work, we will analyze the situation of small elliptically shaped sensors for the detection and position determination of magnetic particles. The results presented should help to guide the design of new sensor layouts for different detection applications.

2. Governing equations

A magnetic volume of magnetization $\boldsymbol{M}$ creates a magnetic field $\boldsymbol{H}$ that can be expressed by a scalar potential ϕ in the form $\boldsymbol{H} = -\nabla\phi$ if no external current densities can be found in the system. The potential ϕ can be calculated solving the Maxwell equations, leading to

$$\Delta\phi = \nabla \boldsymbol{M} \ . \tag{1}$$

The norm of $\boldsymbol{M}$, the saturation magnetization M_S, is a constant depending on the magnetic material considered. Further, we will denote by $\hat{\boldsymbol{m}}$ the normalized direction vector of $\boldsymbol{M}$. The dynamic behaviour of ferromagnetic material is described by the empirical Landau-Lifshitz-Gilbert (LLG) equation

$$\frac{\partial \hat{\boldsymbol{m}}}{\partial t} - \alpha \hat{\boldsymbol{m}} \times \frac{\partial \hat{\boldsymbol{m}}}{\partial t} = \gamma \hat{\boldsymbol{m}} \times \boldsymbol{H}_{\text{eff}} \tag{2}$$

with the phenomenological damping coefficient α and the gyromagnetic ratio γ. The effective magnetic field $\boldsymbol{H}_{\text{eff}}$ decomposes into different contributions:

$$\boldsymbol{H}_{\text{eff}} = \frac{2A}{\mu_0 M_S}(\nabla \hat{\boldsymbol{m}})^2 + \frac{\delta f_{\text{ani}}(\hat{\boldsymbol{m}})}{\delta \hat{\boldsymbol{m}}} + \boldsymbol{H}_{\text{demag}} + \boldsymbol{H}_{\text{ex}} \tag{3}$$

The first summand originates from the exchange energy which favors parallel alignment or more exactly small curvature of each component $\hat{m}_i$. The material depending exchange constant A is a measure for the "stiffness" of the magnetic distribution. The higher the value the less magnetic domains can be found. The second is attributed to magnetocrystalline anisotropy with the anisotropy constant K. Several axes within the material can be energetically preferred due to the microscopic atomic structure. The form of the energy functional f_{ani} depends on the type of anisotropy. The demagnetization field $\boldsymbol{H}_{\text{demag}}$ is the magnetic field along the magnetic layer that is created by the layer itself. We will obtain this contribution as a solution of equation (1). It should be pointed out that this term is of non-

local nature; its value depends on the magnetic field in the whole space. Therefore its calculation requires modeling the area around the magnetic material as well. Finally, all remaining field contributions for instance particle stray fields are summed up in the external field $\boldsymbol{H}_{\text{ext}}$.

Magnetic layers interact by their stray field. However, other coupling effects need to be considered depending on the type of the non-magnetic spacer layer. If a conducting layer is analyzed the so called RKKY-coupling is the main contribution. Its strength as well as its sign oscillates in respect to the thickness d of the non-magnetic separation layer. Phenomenologically, it can be described by

$$J_{\text{RKKY}} = -J_1\langle \hat{\boldsymbol{m}}_1, \hat{\boldsymbol{m}}_2\rangle - J_2\langle \hat{\boldsymbol{m}}_1, \hat{\boldsymbol{m}}_2\rangle^2, \quad (4.1)$$

with constants J_1 and J_2 depending on d.

However, in this work we will restrict our analysis to insulating tunneling barriers. In this case the coupling is due to a correlated surface roughness, the so called Néel-coupling. Assuming a sinusoidal structure of period length λ, a height h and an insulator thickness d the coupling energy is given by

$$J_{\text{Néel}} = M_{\text{S}}^2\langle \hat{\boldsymbol{m}}_1, \hat{\boldsymbol{m}}_2\rangle \cdot \frac{\mu_0\pi^2h^2}{\sqrt{2}\lambda}\exp\left(-\frac{2\pi\sqrt{2}d}{\lambda}\right). \quad (4.2)$$

Néel-coupling favors parallel alignment opposite to stray field coupling. Which effect dominates depends on the size of the sensor. For sensor sizes larger than 1 μm^2 Néel-coupling becomes important, for smaller ones the stray field is the dominant effect.

Transport through the insulating barrier occurs due to tunneling electrons; the tunneling current varies with external fields applied. This effect was first observed by M. Julière in 1975 in Fe/GeO/Co-junctions. The resistance change due to an external magnetic field, the tunneling magnetoresistance (TMR) ratio, can be calculated according to the formula[6]

$$\text{TMR} = \frac{1}{3}\frac{1-\langle\alpha\rangle}{1+\langle\alpha\rangle/3},$$
$$\langle\alpha\rangle = \frac{1}{A_{\text{layer}}}\int_{A_{\text{layer}}}\cos(\measuredangle(\hat{\boldsymbol{m}}_1,\hat{\boldsymbol{m}}_2))\,d\boldsymbol{r}, \quad (5)$$

denoting the sensor area by A_{layer}.

The description of magnetic particles depends on their size. Particles of a diameter ~ 100 nm are single domain particles; they can be approximated by a homogeneously magnetized sphere of magnetic moment $\boldsymbol{m}_{\text{part}}$. Thus, their stray field $\boldsymbol{H}_{\text{stray}}$ at a point $\boldsymbol{r} = r\hat{\boldsymbol{r}}$ is given by the dipolar formula

$$\boldsymbol{H}_{\text{stray}}(\boldsymbol{r}) = \frac{1}{4\pi}\cdot\frac{3\langle \boldsymbol{m}_{\text{part}}, \hat{\boldsymbol{r}}\rangle\hat{\boldsymbol{r}} - \boldsymbol{m}_{\text{part}}}{r^3} \quad (6)$$

where $\langle\cdot,\cdot\rangle$ denotes the Euclidean inner product. If several particles are interacting, their dynamics need to be described in a similar manner to (1). However, since no domain structure is expected, the magnetic moment distribution is constant on the particle volume. Therefore, the first summand in (2) is zero, exchange contributions can be omitted. The resulting equation does not depend on space any longer and (1) reduces to a set of ordinary differential equations. Assuming an N-particle problem, the dynamic equations can be written in the form

$$(Id - \alpha\mathcal{M})\frac{\partial\hat{\boldsymbol{m}}}{\partial t} = \gamma\mathcal{M}\boldsymbol{H}_{\text{eff}} \quad (7)$$

with the blockdiagonal matrix $\mathcal{M}$

$$\mathcal{M} = \begin{pmatrix} \mathcal{M}_1 & & 0 \\ & \ddots & \\ 0 & & \mathcal{M}_{\text{N}} \end{pmatrix}$$

where $\mathcal{M}_{\text{n}} = \varepsilon_{\text{ijk}}\hat{m}_{\text{n,j}}$, $n = 1, \ldots, N$, and the vectors

$$\frac{\partial\hat{\boldsymbol{m}}}{\partial t} = \frac{\partial}{\partial t}(\hat{m}_{\text{x,1}}, \hat{m}_{\text{y,1}}, \hat{m}_{\text{z,1}}, \hat{m}_{\text{x,2}}, \ldots)^T$$
$$\boldsymbol{H}_{\text{eff}} = (H_{\text{eff,x,1}}, H_{\text{eff,y,1}}, H_{\text{eff,z,1}}, H_{\text{eff,x,2}}, \ldots)^T.$$

Equations (1) and (2) together with the additional energy term (4.2) have been implemented via weak form modeling. The ODE-system (7) was integrated as additional ODEs. The model setup is done by a COMSOL plug-in (see Appendix).

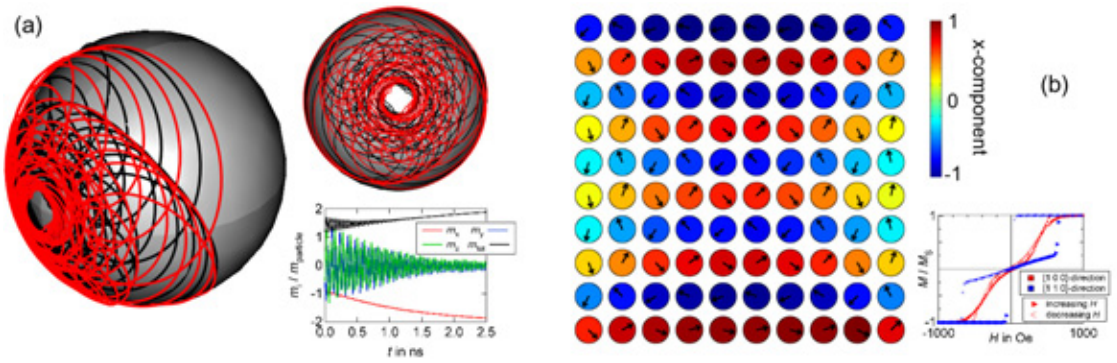

FIG. 1: Examples for the behaviour of magnetic single domain nanoparticles. Subplot (a) shows the dynamics of two 20 nm particles with of a distance of 25 nm, a saturation magnetization M_S = 1000 kA/m and a damping coefficient $\alpha = 10^{-2}$. The lines on the sphere give the trajectories of each magnetic moment vector, the plot the magnetization dynamics. (b) presents the equilibrium of a 10 × 10-particle lattice. The particle state shows an antiferromagnetic configuration which is obtained for $\boldsymbol{H}_{ext} = 0$, the graph shows its hysteresis behaviour for different field directions.

3. Examples for the isolated systems

To get a better impression of the behaviour of each part of the combined system, we will discuss two examples for the single components.

3.1 Two dimensional particle arrays

The dynamics of interacting dipoles occur on a nanosecond timescale. Fig. 1(a) shows the typical behaviour of two single domain particles for a damping constant α = 0.01, which is a common assumption and also a reasonable value for real magnetic materials. The magnetization orientations oscillate strongly until a parallel alignment is achieved.

Self assembled systems of nanoparticles have been thoroughly studied during the last years. Here, we will give an example of their complex magnetization reversal due to dipole-dipole interactions. In the equilibrium state of the two dimensional cubic 10×10-lattice shown in Fig. 1(b) with no external field, magnetic moments align in an antiferromagnetic manner, leading to a very small stray field. Though they do not form magnetic domains, they still show a hysteretic behaviour as shown in the subplot of Fig. 1(b). However, the calculated magnetization curves differ from those obtained for ferromagnetic materials: close to $\boldsymbol{H}$ = 0 the antiferromagnetic ordering is stable against small perturbations, thus, the magnetic susceptibility

$$\chi = (\partial M / \partial H)_{H=0}$$

is very small as seen in Fig. 1. The hysteretic behaviour strongly depends on the direction of the applied magnetic field. If the external field overcomes the inter particle coupling several features like sudden jumps can be found.[7]

3.2 A micromagnetic trilayer

As an example for the dynamics of magnetic layers, we calculate the behavior of a trilayer system (Fig. 2). Three magnetic 100 nm × 100 nm square layers with a thickness of 10 nm each are spatially separated by insulators of also a thickness of 10 nm. We assume the top layer to have a very low exchange constant of $A = 10^{-12}$ J/m, whereas for the centre and the bottom layer we choose $A = 10^{-11}$ J/m. As an initial condition, we set the magnetization configuration parallel to the x-axis in all three ferromagnetic layers.

As the system evolves, different behaviour can be observed: the top electrode forms a so called vortex state, thus, minimizing the energy of its magnetic stray field. Due to their exchange contribution, similar configurations are not possible for the lower layers; they form so called S- and C-states. It may be pointed out that for small geometries as discussed here stray field coupling between layers is a major contribution. This can be seen in Fig. 2: magnetic streamlines

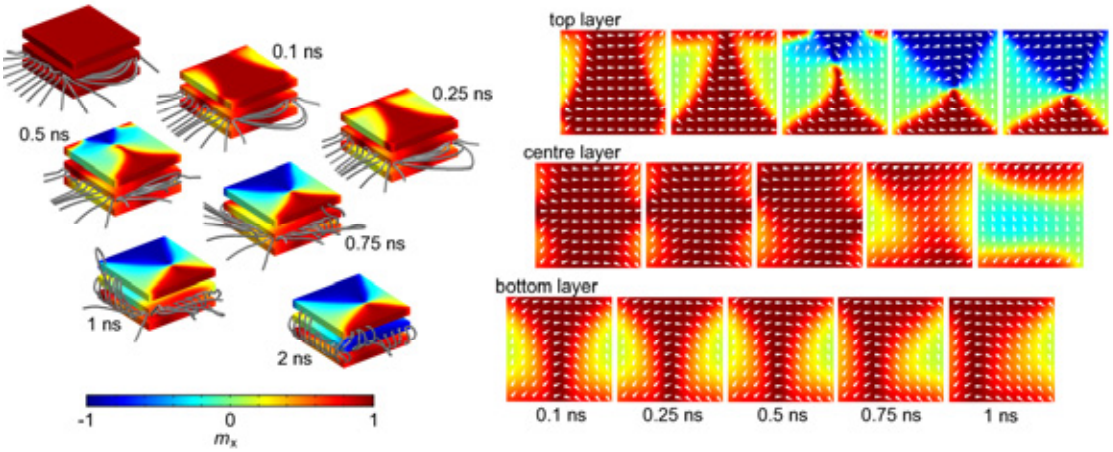

FIG. 2: Dynamic magnetization behaviour of a magnetic trilayer system. Starting from the initial state $m_x = 1$ for all layers, the system evolution is shown on the right side. Since different material parameters are used each layer reaches a different end state: the soft magnetic top electrode creates a vortex state which is not possible for the hard magnetic bottom layers; they form S-states (centre) and C-states (bottom) instead. The behaviour of the external magnetic field is shown on the left side (grey lines); the final configuration leads to an almost vanishing layer stray field.

run between neighboring layers, minimizing the total stray field energy.

4. Combined system

The actual setup of the combined system depends on the measuring task. Here we want to focus on two different objectives: (a) detection that determines the position of a single magnetic particle and (b) detection that measures the number of particles on top of the multilayer system. The setup discussed is schematically shown in Fig. 3: the sensor consists of two 4 nm-CoFeB-layers separated by a tunneling barrier of 2 nm. Its shape is elliptic with axis lengths of 400 and 100 nm. We do not want to focus on the reason for this specific shape choice, for more information see ref.[5] The material parameter chosen are $M_S = 1194$ kA/m and $A = 2.86 \cdot 10^{-11}$ J/m which are the material parameters for CoFeB. It should be pointed out that the dynamics of the magnetic layers are not important for the measuring tasks described; instead a stationar solution would be sufficient. However, stationary system solvers usually do **not** converge as long as the initial guess is not close to the end state. To obtain a good initial guess a combination of solvers should be used: (a) calculate a number of time steps with a transient solver and (b) use this for the initial guess to obtain a stationar solution. This strategy usually succeeds, the number of time steps though differ in respect to the regarded system, but may be estimated by the material parameters and the geometry dimensions.

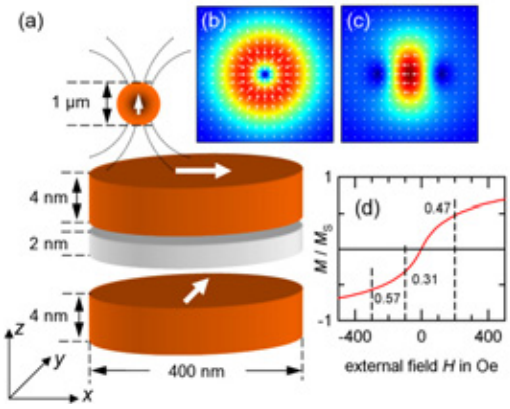

FIG. 3: (a) Schematic of the sensor layout, two soft magnetic layers are separated by an insulator. (b) and (c) show the in-plane components of a magnetic particle aligned in z- and in x-direction, respectively. The magnetization behaviour is shown in (d).

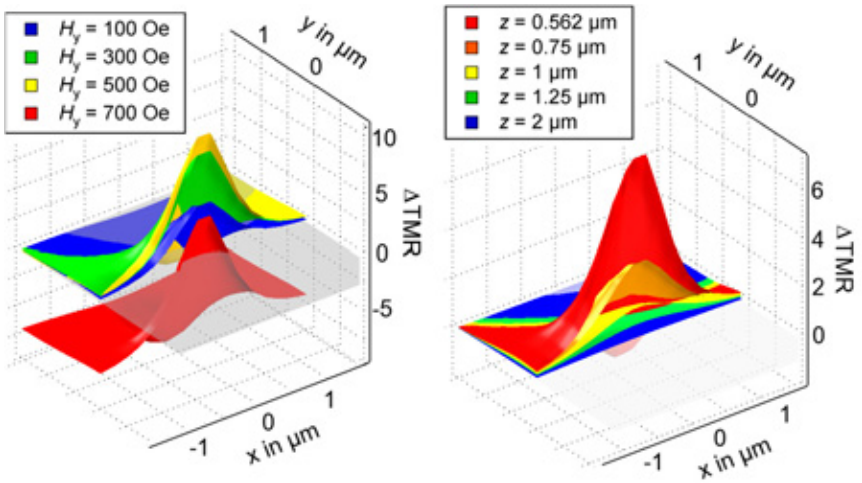

FIG. 4: Cut of the ΔTMR-maps calculated at the grid points according to (8) for (a) different external field values and (b) particles at different heights. The grey level indicate the plain ΔTMR = 0. Particle saturation is chosen according to Fig. 3(d).

4.1 Single particle detection

Magnetic particles close to the soft magnetic top layer exert a torque to the magnetization distribution at every point of the layer its size depends on the position of the particle; therefore, particles at different positions lead to a different sensor signal, as long as the particle diameter is at the same size scale as the sensor size. In this regime, the sensor can be used to estimate the particle position. We consider a magnetic sphere of r = 500 nm with a saturation magnetization of 120 kA/m. The area around the sensor is discretized by a finite grid with grid coordinates

$$\begin{aligned} x &= -1.5\mu m + (i-1)\cdot 0.2\mu m\,, \\ y &= -1.5\mu m + (j-1)\cdot 0.1\mu m\,, \\ z &= 0.562\mu m\,. \end{aligned} \qquad (8)$$

with i = 1, … 16, and j = 1, … , 31. The z-coordinate originates from the estimation of the minimum height possible, decomposing into the particle radius and a passivation layer on top of the sensor of around 62 nm. The response of the sensor can be calculated using formula (5). To ease the comparison between different configurations, we evaluate the relative ratio

$$\Delta\mathrm{TMR} = \frac{\mathrm{TMR}_{\mathrm{part}} - \mathrm{TMR}_{\mathrm{free}}}{\mathrm{TMR}_{\mathrm{free}} + 1}\,, \qquad (9)$$

where $\mathrm{TMR}_{\mathrm{free}}$ and $\mathrm{TMR}_{\mathrm{part}}$ denote the resistance changes without and with a particle, respectively. Results for a particle aligned along the y-direction are presented in Fig. 4 for different field strengths. We find an increasing response of the sensor with increasing applied field strength as long as a critical value (≈ 700 Oe) is not exceeded. However, the TMR value itself decreases, therefore, the resolution increase in respect to space is obtained at the price of a smaller field of visibility.[8] This effect is comparable to the focus setting of optical lenses.

Further, Fig. 4(b) shows the influence of the distance between particle and sensor. The obtained response decreases rapidly, which is due to a $1/r^3$-dependence of the particle stray field (6). At around a distance of twice the particle radius, the measurable signal is commonly below the noise signal of such devices. Especially for the detection of particles in continuous flow devices, this is a severe restriction. For examples on strategies to increase the detection threshold see *Observation of Magnetic Particles in Continuous Flow Devices by Tunneling Magnetoresistance Sensors*, in the current conference proceedings. Since the sensor response depends on the particle position as shown in Fig. 4 a space resolute detection is in general possible. Due to identical signals at different positions the method needs to be improved by e.g. employing sensor arrays.

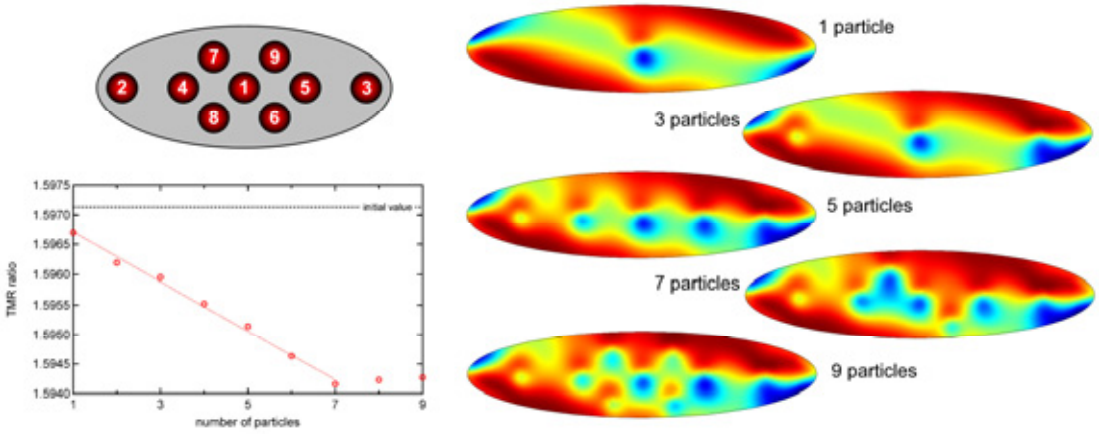

FIG. 5: Effect of multiple particles on the magnetization distribution. Particles of a magnetization M_S = 1000 kA/m and a radius of r = 5 nm are placed on top of the sensor. The external field is chosen in z-direction. As long as particles are placed far enough part from each other the sensor response adds up linearly. For small distances the effects interfere, the signal dependence changes.

4.2 Multiple particle effects

If a certain number of particles is close to the sensor, the obtained response changes. We will assume particles of saturation magnetization of M_S = 1000 kA/m and a radius r = 5 nm that are placed on top to the sensor according to positions given in Fig. 5. The sensor plot show the x-component of the magnetization, the positions of the particles can clearly be identified. As long as the magnetic objects have a sufficiently high distance from each other (approximately a distance of twice the particle diameter) the resulting TMR-response behaves linearly. In this regime the sensor enables a particle number detection; every data value corresponds to a single particle number. For higher sensor coverage saturation can be observed; the critical degree of coverage depends on the parameters of the magnetic layer.

If the external magnetic field is changed during the measurement, the dipolar coupling of the magnetic particles can indirectly be observed for sufficiently high sensor coverage. Fig. 6 shows the TMR-response of the sensor for 14 nm Co-particles that are immersed in a field ranging from -250 up to 250 Oe. The coupling of the particles leads to a hysteretic behaviour of the total magnetic system. The model predicts a change of coupling depending on the sensor coverage that can be verified in experiments[9].

5. Conclusion and Outlook

We have implemented the dynamic equations for micromagnetism coupled to single domain particles into COMSOL Multiphysics. Our model enables the calculations of the properties and of magnetoresistive sensors and is well suited for the design guidance of new sensor layouts or array configurations. The main goal is the amplification of the resolution in respect to spatial detection as well as number evaluation. Different strategies pursued at the moment are contained in the paper *Dynamic Observation of Magnetic Particles in Continuous Flow Devices by Tunneling Magnetoresistance Sensors*, in the current conference proceedings.

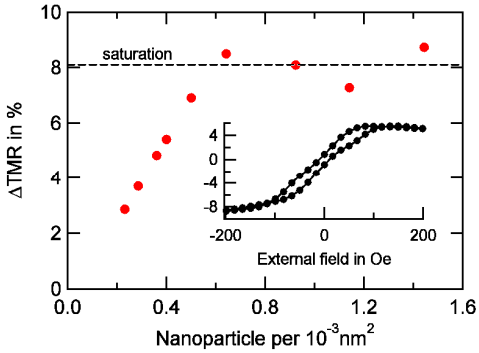

Fig. 6: Indirect observation of the dipolar particle coupling for different degree of sensor coverage.

Acknowledgements

The authors would like to thank the SFB 613 for financial support in the framework of the project K3.

Appendix

The number of equations needed for the model definition results in an amount of plain text that easily exceeds several 1000 characters making it impossible to implement via the COMSOL GUI. In the framework of our studies, we therefore developed the COMSOL plug-in PADIMA (Fig. 7) that sets up all the equations for all the above mentioned tasks, as well as for other applications e.g. frequency-resonance analysis of particle arrays, moving particles in rotating fields and their influence on sensor / sensor arrays, dynamic particle detection or multilayers under high external stresses combining micromagnetic equations with structural mechanics in ALE-frameworks. Material libraries are also implemented. For further information contact the corresponding author.

Literature

[1]A. Weddemann, B. Eickenberg, F. Wittbracht, A. Auge, A. Hütten, J. Appl. Phys. **106**, 024510 (2009)
[2]A. Weddemann, F. Wittbracht, A. Auge, A. Hütten, Microfluid Nanofluid DOI 10.1007 / s10404-009-0473-y
[3]A. Weddemann, F. Wittbracht, A. Auge, A. Hütten, Appl. Phys. Lett. **94**, 173501 (2009)
[4]A. Auge, A. Weddemann, F. Wittbracht, A. Hütten, Appl. Phys. Lett. **94**, 183507 (2009)
[5]C. Albon, A. Weddemann, A. Auge, K. Rott, A. Hütten, Appl. Phys. Lett. **95**, 023101 (2009)
[6]W. Schepper, J. Schotter, H. Brückl, G. Reiss, J. Biotechnol, **112**, 35 (2004)
[7]A. Weddemann, A. Auge, F. Wittbracht, D. Kappe, A. Hütten, submitted to JMMM
[8]A. Weddemann, A. Auge, F. Wittbracht, C. Albon, submitted to NJP
[9]C. Albon, A. Weddemann, A. Auge, D. Meißner, P. Jutzi, K. Rott, A. Hütten, submitted to APL

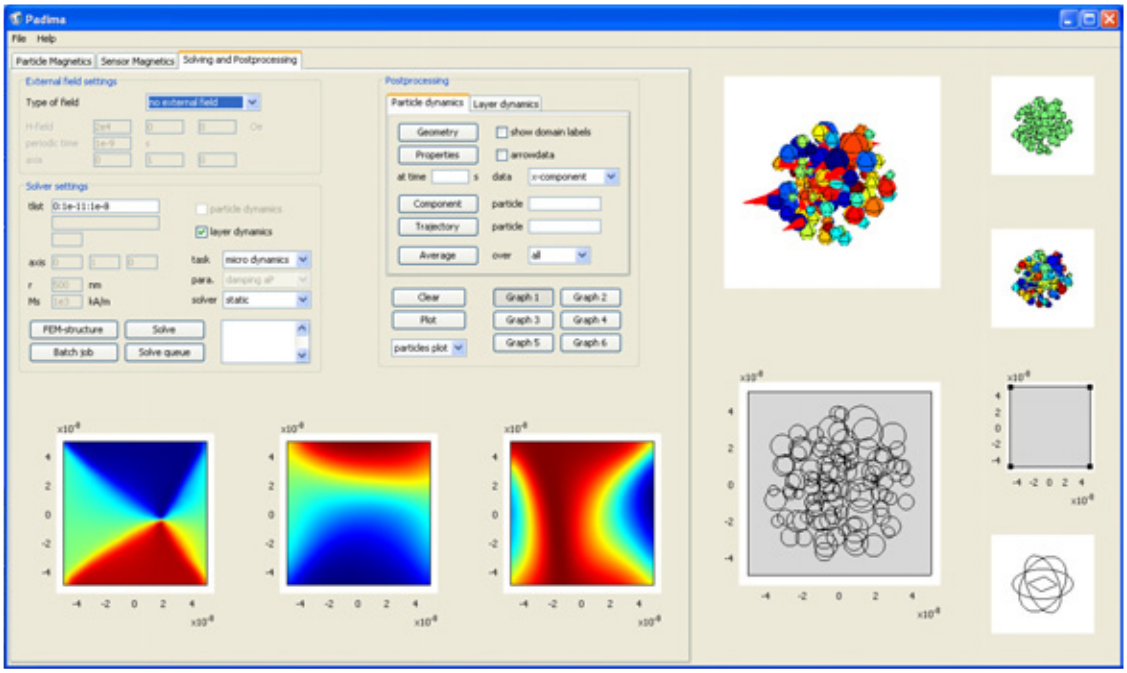

FIG. 7: Graphical user interface for the model setup enabling various applications.